A numerical study of variability in the North Icelandic Irminger Current

Jian Zhao[1], Jiayan Yang[1], Stefanie Semper[2], Robert S. Pickart[1], Kjetil Våge[2], Hedinn Valdimarsson[3], Steingrimur Jonsson[4]

1, Woods Hole Oceanographic Institution, Woods Hole, Massachusetts, USA
2, Geophysical Institute, University of Bergen and Bjerknes Centre for Climate Research, Bergen, Norway

3, Marine and Freshwater Research Institute, Iceland

4, Marine and Freshwater Research Institute and University of Akureyri, Iceland

Corresponding author: Jian Zhao (jzhao@whoi.edu)

Key Points:

The water mass over the entire north Icelandic shelf exhibits strong seasonal variations in both velocity and hydrography.

The wind stress southwest of Iceland is mostly responsible for the interannual variations in the Atlantic Water transport and salinity.

Temperature changes on the north Icelandic shelf, however, are equally attributable to the buoyancy flux and wind forcing.

Abstract

The North Icelandic Irminger Current (NIIC) is an important component of the Atlantic Water (AW) inflow to the Nordic Seas. In this study, both observations and a high-resolution (1/12°) numerical model are used to investigate the seasonal to interannual variability of the NIIC and its forcing mechanisms. The model-simulated velocity and hydrographic fields compare well with available observations. The water mass over the entire north Icelandic shelf exhibits strong seasonal variations in both temperature and salinity, and such variations are closely tied to the AW seasonality in the NIIC. In addition to seasonal variability, there are considerable variations on interannual time scales, including a prominent event in 2003 when the AW volume transport increased by about 0.5 Sv. To identify and examine key forcing mechanisms for this event, we analyzed outputs from two additional numerical experiments: using only the seasonal climatology for buoyancy flux (the momentum case), and using only the seasonal climatology for wind stress (the buoyancy case). It is found that changes in the wind stress are predominantly responsible for the interannual variations in the AW volume transport, AW fraction in the NIIC water, and salinity. Temperature changes on the shelf, however, are equally attributable to the buoyancy flux and wind forcing. Correlational analyses indicate that the AW volume transport is most sensitive to the wind stress southwest of Iceland.

1 Introduction

The transport of warm and saline Atlantic Water (AW) over the Greenland-Scotland Ridge (GSR) into the Nordic Seas is an essential component of the Atlantic Meridional Overturning Circulation (*Dickson et al.* 2008). A total transport of about 8.5 Sv of AW is distributed among three branches across the GSR: about 0.8 Sv through the Denmark Strait; about 3.8 Sv between Iceland and the Faeroe islands (IF), and about 3.8 Sv through the Faroe-Shetland Channel (FSC) (*Østerhus et al.* 2005; *Hansen et al.* 2015). The AW inflow results in considerable fluxes of heat, salt and nutrients into the Nordic Seas and ultimately the Arctic Ocean, affecting the high-latitude climate, water transformation, and ecosystem (*Dickson and Brown*, 1994; *Hansen and Østerhus*, 2000; *Dickson et al.* 2008; *Hansen et al.* 2003; 2010, 2015).

The northward transport of the AW through the Denmark Strait occurs mainly via the North Icelandic Irminger Current (NIIC), whose origin can be traced to the Irminger Current in the subpolar North Atlantic Ocean. The NIIC flows northward on the eastern side of the Denmark Strait (Fig. 1). The warm and saline AW in the NIIC meets the cold and low-salinity Polar Water (PW) off Iceland's northwest coast. A mixture of AW and PW is further fluxed onto the north Icelandic shelf. The NIIC, even with a relatively small volume transport, is also a main source of heat and salt to the Iceland Sea and thus strongly influences the convection processes there. *Våge et al.* (2011) suggested that the AW in the NIIC is fluxed offshore by eddies and cooled by air-sea flux to form a dense water mass that feeds the North Icelandic Jet (NIJ) – an upstream branch of the Denmark Strait Overflow. The existence of this local overturning loop has been supported by numerical simulations (*Behrens et al.* 2017). North of Iceland the NIIC continues to flow anti-cyclonically over the outer part of the shelf. The flow is favorable for the migration of larval cod from the main spawning grounds south of Iceland to the nursery places on the north Icelandic

shelf (*Jónsson and Valdimarsson* 2005). The relatively high nutrient content in the AW is also important for primary productivity around Iceland (*Thordardottir*, 1984).

Given the importance of the NIIC to the local climate and ecosystem, considerable efforts have been devoted to monitor the NIIC variability using both ships and long-term moorings. The Hornbanki section on the north Icelandic shelf is the most well maintained mooring array that has been continuously measuring the NIIC since 1994. As a result, the mean structure and variations of the current are well documented at that location (e.g., *Kristmannsson* 1998; *Jónsson and Valdimarsson* 2005; 2012; *Østerhus et al.* 2005). The long-term mean volume flux of AW in the NIIC has been estimated to be 0.88 Sv and displays substantial variability on multiple time scales (*Jónsson and Valdimarsson* 2012). In addition, the NIIC volume transport has been shown to co-vary with the transports of the other two branches of the AW inflow. For instance, a negative correlation between the NIIC and the FSC transports was detected in both model and observational data (*Nilsen et al.*, 2003; *Østerhus et al.*, 2005).

Among the three branches of the AW inflow to the Nordic Seas, the NIIC is by far weakest in terms of volume transport, and arguably the least studied (e.g. *Nilsen et al.* 2003; *Olsen and Schmitch.* 2007; *Richter et al.*, 2009; *Sandø et al.* 2012). There remains considerable uncertainty regarding the processes and mechanisms that are responsible for its variability. To date, several mechanisms have been identified that appear to influence the overall the overall transport of the AW across the GSR, including: wind-induced wave propagation from the Atlantic Ocean into the Nordic Seas (*Orvik and Skagseth*, 2003; *Sandø and Furevik*, 2008); local wind forcing driving the transport in the FSC (*Sherwin et al.* 2008; *Richter et al.*, 2012); and the AW inflow compensating the overflow (*Hansen et al.* 2010; *Sandø et al. 2012*). Among these processes, the large-scale wind forcing, especially the North Atlantic Oscillation (NAO), has been shown to

play a key role (*Nilsen et al.* 2003; *Olsen and Schmitch.* 2007; *Richter et al.* 2009). In addition, changes in the pattern and strength of the subpolar gyre have also been linked to the AW transport into the Nordic Seas (*Hátún et al.* 2005; *Hakkinen et al.* 2011).

The seasonal cycle for the AW transport carried by the NIIC is distinct, with a minimum in late-spring and maximum in summer (*Jónsson and Valdimarsson* 2012). This seasonal variability is considerably different from that in the FSC and IF. For instance, the AW inflow in the IF is strong in early-spring and weak in late-summer to early-fall (*Hansen et al.*, 2008). This indicates that the dynamics for the NIIC may be different from the other two branches. The model simulations of *Logemann and Harms* (2006) showed that most high-frequency (time scales ranging from days to months) and seasonal NIIC variability are linked to the local wind around Iceland. It is unclear whether the same processes and forcing are responsible for interannual variability, such as the large anomalous transport observed in 2003 (*Jónsson and Valdimarsson*, 2012). The measurements analyzed by *Logemann and Harms* (2006) spanned the period between May 1997 and June 2002, and therefore excluded the anomalous event in 2003.

This study investigates the structure and variability of the NIIC using a high-resolution (1/12°) numerical model. Several model runs have been conducted to examine the causes for interannual changes in the NIIC. Our experiments are designed to separate the relative contributions from wind stress and buoyancy forcing to the seasonal and interannual variability. The model setup, including the boundary conditions and forcing fields, are explained in section 2. The model simulations and analyses are presented and discussed in section 3. Further discussion and a summary are then presented in Section 4.

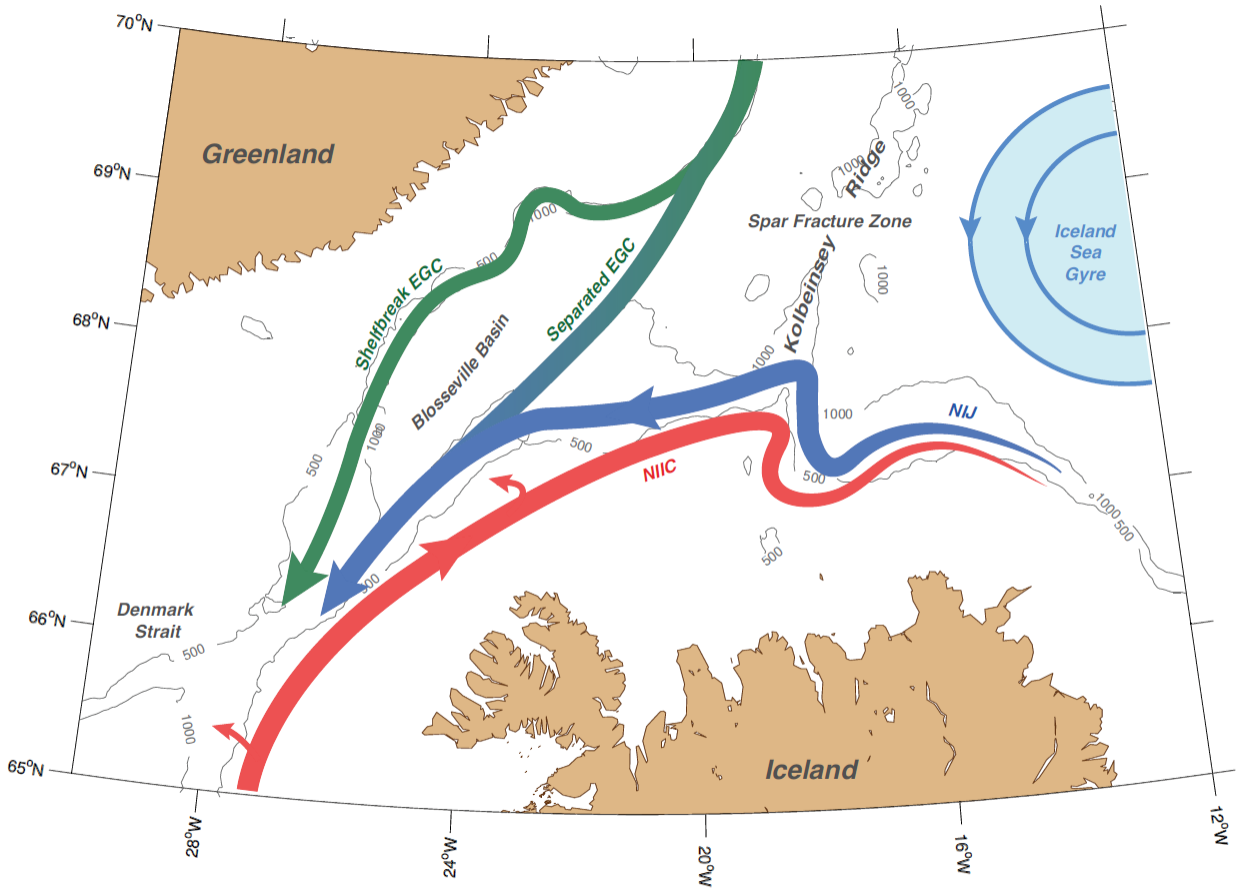

Figure 1. Schematic circulation in the region north of Denmark Strait and geographic place names, after Våge et al. (2013). The 500 m and 1,000 m isobaths are contoured in gray. EGC, East Greenland Current; NIIC, North Icelandic Irminger Current; NIJ, North Icelandic Jet.

2 Data and model

2.1 Observations

The mooring data used in this study come from a series of deployments of the Hornbanki array (Fig. 2). The reader is referred to *Jonsson and Valdimarsson* (2012) for a description of the configuration of moorings, the instrumentation employed, and the data coverage. Here we use the AW transport timeseries, which is the fraction of the total transport associated with warm and salty AW, computed using an end-member analysis (see *Jonsson and Valdimarsson* (2012) for details).

The shipboard data come from a series of 10 occupations of the Hornbanki section that included both conductivity-temperature-depth (CTD) measurements and lowered acoustic Doppler profiler (LADCP) measurements. In all instances the CTD conductivity data were calibrated using in-situ water samples, and the LADCP data were de-tided. The reader should consult *Pickart et al.* (2017) for details of this, including measurement accuracies. The occupations occurred in Oct. 2008, Aug. 2009, Aug. 2010, Feb. 2011, Sep. 2011, Feb. 2012, Aug. 2012, Aug. 2013, Aug. 2015 and Aug. 2017.We constructed mean vertical sections of potential temperature, salinity, and absolute geostrophic velocity (perpendicular to the section[1]) to be compared with the model output.

Satellite data are used to further validate the model and to supplement our analyses. They include the Absolute Dynamic Topography (ADT) and surface geostrophic velocity fields between 1992 and 2015. The Ssalto/Duacs altimeter products are produced and distributed by the Copernicus Marine and Environment Monitoring Service (CMEMS) (http://www.marine.copernicus.eu).

[1] Since the section is oriented north-south, the absolute geostrophic velocity is zonal.

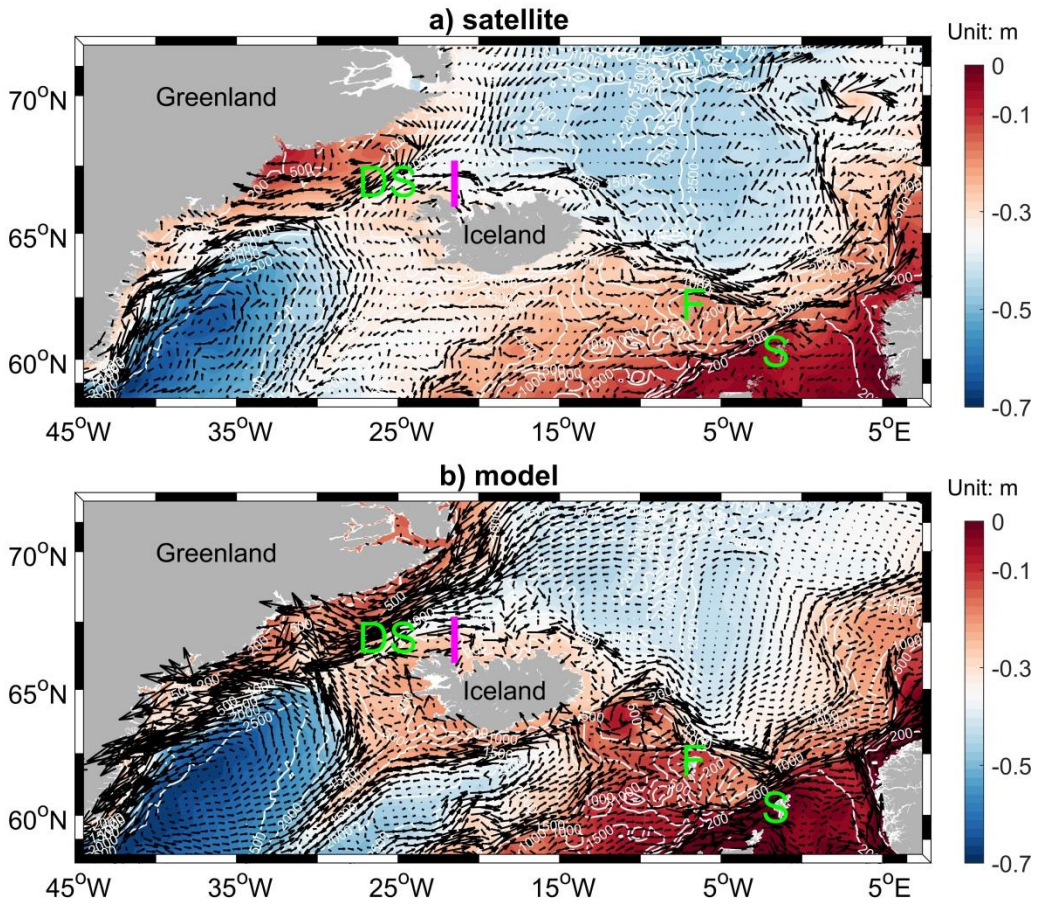

Figure 2. Mean surface geostrophic circulation from satellite altimetry observations and the HYCOM control experiment. The long-term mean (1993-2015) absolute dynamical topography (ADT) observed by the satellite altimetry (color) is shown in a). The mean sea surface height simulated by HYCOM is displayed in b). The surface geostrophic currents calculated from altimetry and HYCOM and are shown by the gray vectors. The bathymetric contours (white lines) indicate isobaths of 200m, 500m, 1000m, 1500m, 2000m and 2500m. DS denotes Denmark Strait. F and S represent Faroe and Shetland, respectively. The magenta lines denote the Hornbanki section.

2.2 Numerical Model

Numerical simulations were performed using an eddy-resolving high-resolution (1/12°) configuration of the HYbrid Coordinate Ocean Model (HYCOM). The model was originally configured by *Xu et al.* (2010) and used in several studies in both the Atlantic Ocean and Nordic Seas (*Xu et al.* 2010; 2012; 2013). The model domain spans from 28°S to 80°N and has 32 vertical layers. The horizontal resolutions range from 3-5 km in the subpolar North Atlantic. Along the northern and southern boundaries we apply the no-normal flow condition in the velocity field and restore the temperature and salinity to their monthly climatological fields. Further details of the model setup are explained by *Xu et al.* (2010; 2012) and therefore not repeated here.

The 1/12° HYCOM simulations were found to successfully reproduce both the long-term mean and variations of the subpolar North Atlantic circulation, particularly the AMOC, the boundary currents in the Labrador Sea, and the North Atlantic Current (*Xu et al.* 2012; 2013). We used the climatological simulation E026 by *Xu et al.* (2012) as an initial condition, from which our regional HYCOM model was further integrated for 25 years by repeatedly using the daily 1992 atmospheric forcing from National Centers for Environmental Prediction (NCEP) Climate Forecast System Reanalysis (CFSR) data. After this 25-year spin-up, three experiments were performed. In the *control* run, the HYCOM was integrated from 1992 to 2015 with daily forcing fields from NCEP CFSR data. In the *momentum* run, the HYCOM was forced by climatological buoyancy flux, but interannually varying momentum fluxes. In the *buoyancy* run, the model was driven by climatological momentum flux, and interannually varying buoyancy flux. The two sensitivity experiments are designed to evaluate the relative contribution from each forcing field – buoyancy or wind stress – to the interannual variations of the NIIC.

3 Results

3.1 Mean and seasonal cycle

The HYCOM *control* experiment reproduces reasonably well the surface circulation in the subpolar North Atlantic (Fig.2). In addition to the topographic-following cyclonic circulation and the East Greenland Current (EGC), the model also simulates reasonably well the three AW inflow branches to the Nordic Seas in the Faroe-Shetland Channel, over the Iceland-Faroe Ridge and on the eastern part of the Denmark Strait. The simulated circulation is broadly consistent with that derived from available observations (e.g. *Valdimarsson and Malmberg*, 1999; *Jakobsen et al.* 2003). The warm and saline water masses are clearly present along the pathways of the three inflow branches (Fig.3), indicating their origins from the Atlantic Ocean. Once in the Nordic Seas the AW is either transformed to dense waters or further transported into the Arctic Ocean.

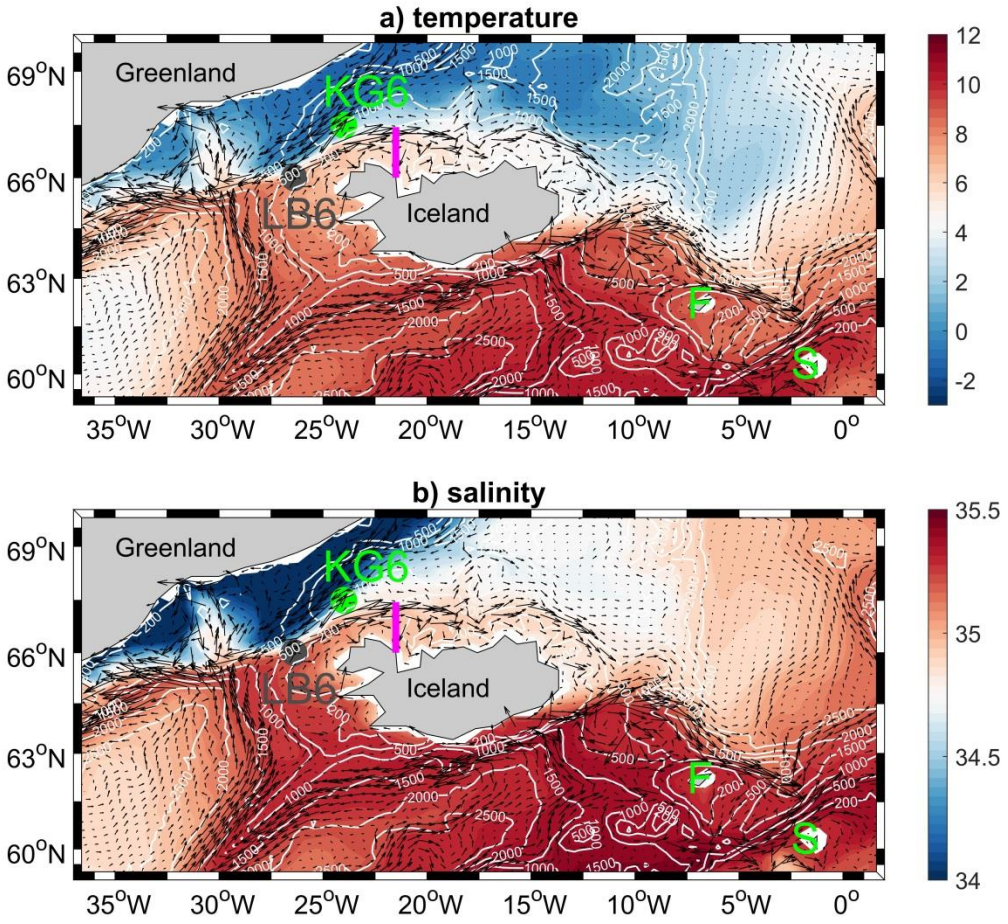

183

184 Figure 3. Mean fields at 110 m simulated by HYCOM for (a) Temperature (°C) and (b) Salinity.
185 The LB6 (station 6 on the Látrabjarg transect) and KG6 (station 6 on the Kögur section) sites are
186 indicated. These are the AW and PW end member locations (see text). Isobaths (white contours)
187 are the same as in Fig. 2.

188

189

190

This study focuses on the NIIC which separates from the Irminger Current in the region to the southwest of Iceland and flows northward then eastward over the outer north Icelandic shelf. We now compare the modeled NIIC at the Hornbanki section to the observations. The measured velocity field along the Hornbanki section indicates that the shelf region with water depths shallower than 300 m is occupied by eastward flow (Fig. 4a). The eastward current has a strong barotropic component inshore of the shelfbreak with significant flow extending from the surface to the bottom. Farther offshore, there is a branch of westward flow toward the Denmark Strait centered near the 600 m isobath. This is the NIJ, which transports overflow water denser than σ_θ = 27.8 kg/m^3 (see also *Jónsson* 1999; *Jónsson and Valdimarsson* 2004; *Våge et al.* 2011; *Pickart et al.* 2017).

The model output, subsampled to the cruise periods, shows consistent structure with the observed velocity fields (Fig. 5a). The model has a well-defined velocity core near the shelfbreak where the density front is located. The maximum velocity in both the observations and the model is more than 0.2 m/s, suggesting that the NIIC is a relatively strong current. While there are no observations south of 66.7°N, the numerical results reveal another branch of eastward velocity in the coastal region. The model also reproduces the westward NIJ on the continental slope, but its amplitude is weaker than the observations. It should be mentioned that the long-term mean fields, averaged over all monthly model outputs between 1992 and 2015, are very similar and not shown here. As such, the fields displayed here accurately reflect the long-term pattern.

The warm and salty AW can be easily identified between the coast and shelfbreak in both the observations and model (Fig.4 and Fig. 5). A layer of low salinity water is located near the surface, likely due to the fact most cruises were performed in summer. The front between the

214 AW and the relatively colder and fresher water offshore is bounded by the σ_θ levels 27.6 and
215 27.9 and is collocated with the eastward flow. Following the method employed by *Jónsson and*
216 *Valdimarsson* (2012) and *Pickart et al.* (2017), we computed the AW fraction across the
217 Hornbanki section for the model output. In particular, we chose the AW and PW end member
218 sites to be at the same geographical locations as those used in the observational studies, denoted
219 by LB6 and KG6, respectively[2], in Fig. 3. The simulated temperature and salinity maps at 110m
220 indicate that indeed the LB6 site is embedded in the AW, and the water mass at KG6 is
221 characterized by the cold and fresh PW (Fig. 3 and Fig. 6). Furthermore, the amplitudes of both
222 the seasonal and interannual variations at KG6 are larger than at LB6 (Fig. 6), which is
223 consistent with observations (*Jónsson and Valdimarsson* 2012). We then computed the fraction
224 of AW at each depth along the Hornbanki section using the corresponding end member
225 temperature and salinity values at LB6 and KG6. Finally, the AW transport across the Hornbanki
226 section was calculated by multiplying the AW fraction, velocity and spatial area for each grid
227 cell in HYCOM.

[2] LB6 is station 6 on the Látrabjarg line and KG6 is station 6 on the Kögur line [*Jonsson and Valdimarsson*, 2012].

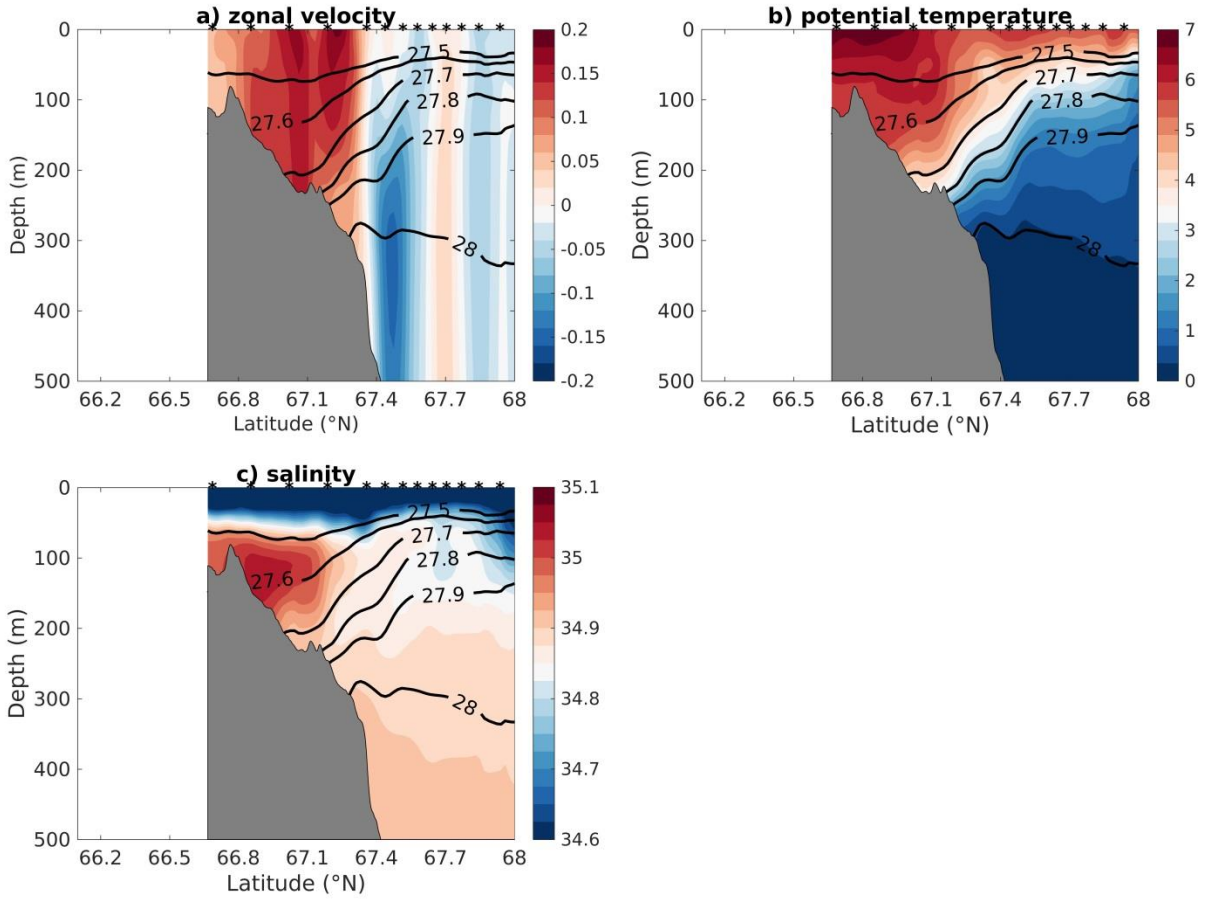

Figure 4. Mean vertical sections along the Hornbanki section from the observations. Zonal velocity (a, unit: *m/s*), temperature (b, unit: ℃) and salinity (c). The potential density (σ_θ, unit: kg/m^3) are denoted by black contours. The average positions of the CTD stations are indicated by asterisks. The average station distance is about 18.5 km on the shelf and about 8 km offshore the shelfbreak.

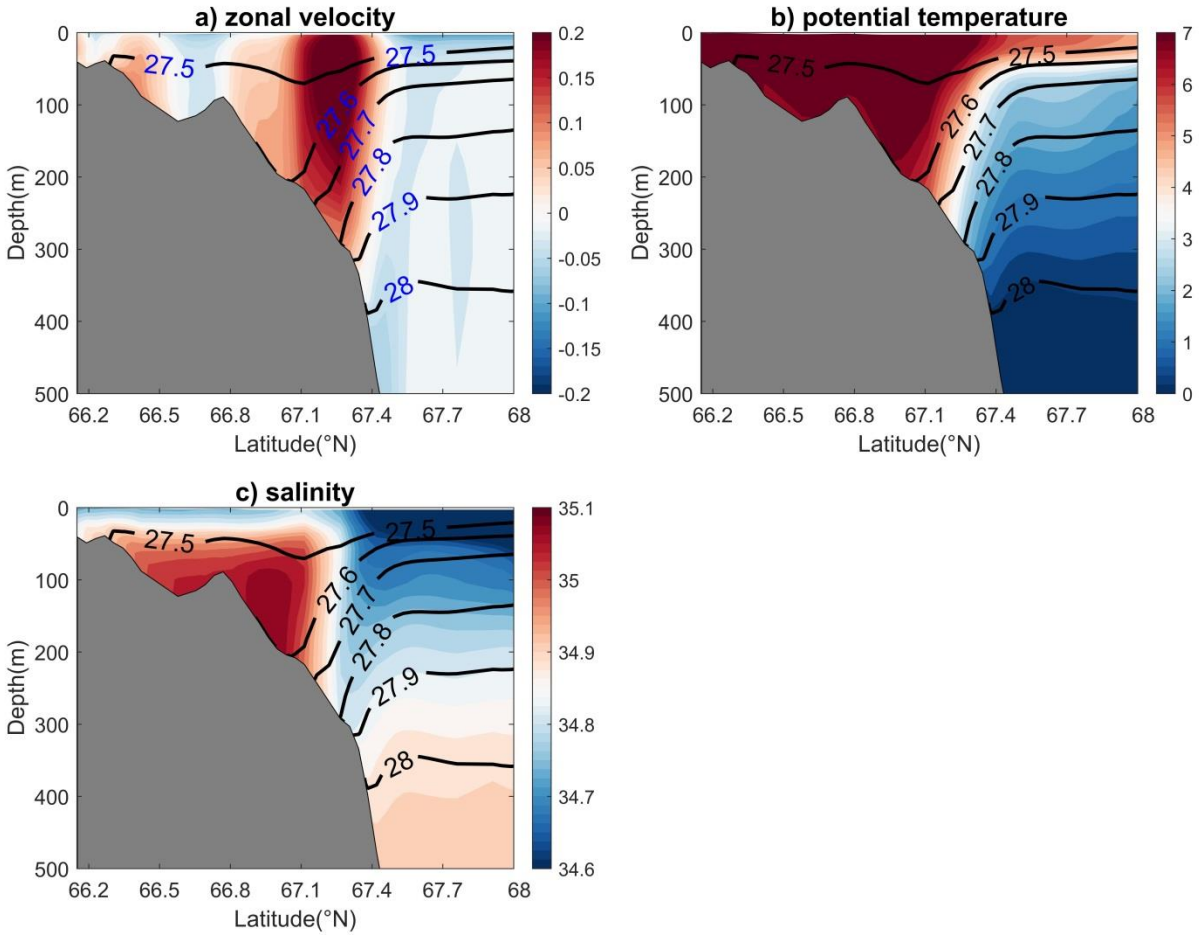

235

236 Figure 5. Same as Fig. 4 except for the Hornbanki section from the HYCOM control experiment.

237 The model outputs are between 1992 and 2015 and the fields correspond to the cruise periods,

238 except the shipboard occupation in Aug. 2017.

239

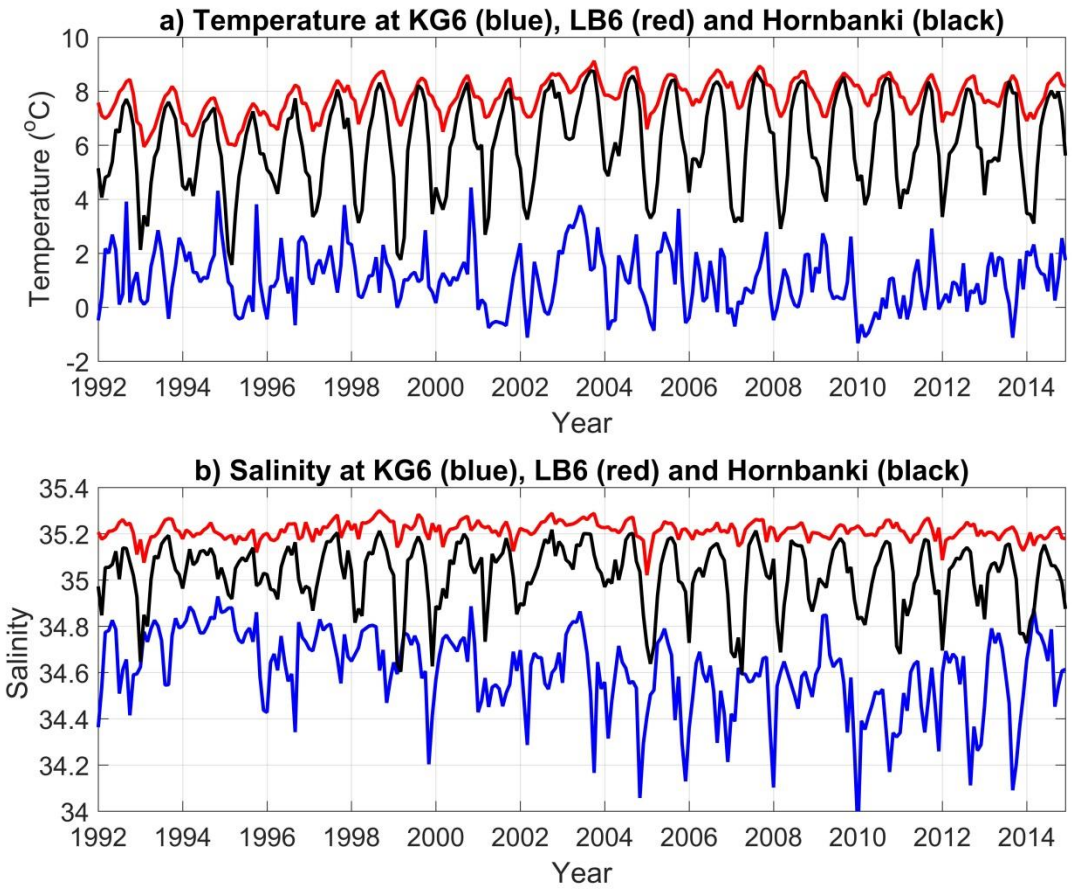

240

241 Figure 6. Temperature (a) and salinity (b) at 110m for the LB6 (red) and KG6 (blue) stations in
242 the HYCOM control run. The black lines denote the temperature and salinity at 110m at the
243 Hornbanki section (67°N).

244

245

246

247

The monthly-averaged total NIIC transport (i.e. not just the AW portion) for the model time period of 1992–2015 reveals a significant amount of variability (Fig. 7a). The long-term mean value is 1.36±0.40 Sv. A 2-year low-pass filter is applied to isolate the interannual signal, which has a range of 1.00 Sv to 1.86 Sv. Fig. 7a also shows the monthly time series of the AW transport in the HYCOM *control* experiment compared with the observations analyzed by *Jónsson and Valdimarsson* (2012). The mean model AW transport is 0.81 Sv compared to the measured value of 0.88 Sv. The correlation coefficient between the model and data is 0.72, which is significant at the 95% confidence level of Student's t test. The standard deviation in the model is 0.40 Sv, slightly larger than that from the measurements, 0.34 Sv. It should be emphasized that the total NIIC transport is about 0.55 Sv higher than the AW volume transport. While both of them have similar standard deviations (0.40 Sv), we now show that their seasonal and interannual characteristics are different.

The monthly climatological seasonal cycle for the total simulated NIIC transport, as well as the AW portion, are presented in Fig. 7b. The total transport reaches a minimum in late-winter and maximum in late-fall. However, the AW component has a more pronounced seasonal cycle which peaks earlier in the fall. This is because the seasonal variation of the AW component reflects the changes in both the velocity and the AW fraction. The seasonal range in AW transport is about 0.75 Sv in HYCOM compared to 0.45 Sv for the total NIIC transport. Therefore, the AW fraction is an important factor to modulate the seasonal variation of the AW transport in the NIIC. The percentage of AW along the model section exhibits a minimum of 50% in March and a maximum of 95% in September.

The observed seasonal cycle for the AW transport is similar to that in the HYCOM *control* experiment (Fig. 7b). Both model results and observations show that the minimum transport

occurs in late winter and the maximum takes place in early-fall. However, there are some differences most notably that the seasonal range is greater in the model (0.75 Sv in HYCOM compared to 0.68 Sv for the observations), and that the measured AW transport decreases more markedly after September. The difference between the modeled and observed seasonal cycles for the AW properties and transports is likely due to the model's deficiency in representing the mixing between AW and PW. For example, the observed maximum proportion of AW occurs in July with a value of 85% (*Jónsson and Valdimarsson* 2012), compared to September with a percentage of 95% in the model. Observational biases may also contribute to the model-data inconsistency. We note that the KB6 and LB6 stations were sampled four times annually, and occasionally missing instruments or moorings on the Hornbanki section cause about 10% - 15% error in the estimation of the AW transport (*Jónsson and Valdimarsson* 2012).

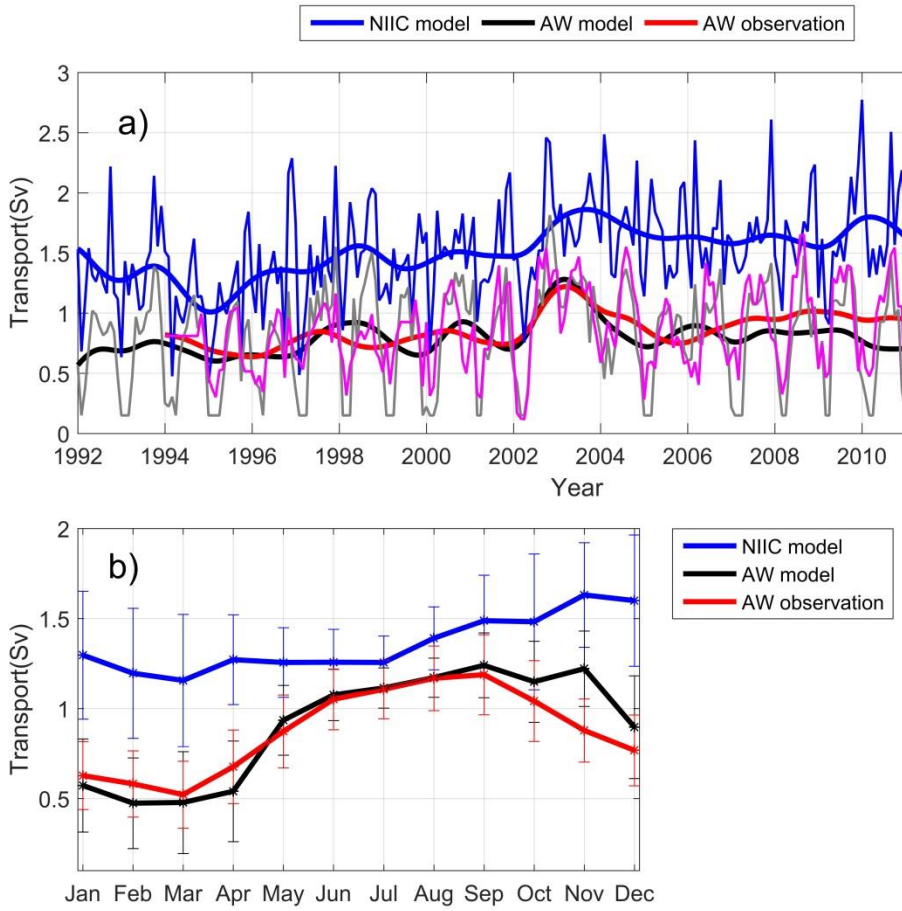

Figure 7. a) Monthly (blue thin line) and 2-year low-pass filtered (blue thick line) time series for the total model NIIC transport (without being weighted by the AW fraction). Also shown are the monthly AW transports of the NIIC across the Hornbanki section in the HYCOM control experiment (gray thin line) and the observation (magenta thin line). The 2-year low-pass time series are indicated as well (black thick line for HYCOM and red thick line for observation). b) Climatological seasonal cycles of the AW transport from HYCOM (black line) and the observation (red line), and that for the total NIIC transport (blue line). The standard deviations are denoted by the thin vertical bars.

294 The spatial structure associated with the seasonally varying NIIC can be identified from the
295 satellite altimetry data (Fig. 8). When the NIIC reaches its minimum and maximum transports in
296 March and September, respectively, the ADT exhibits corresponding negative and positive
297 anomalies along the Iceland coast. The ADT in March is anomalously low over the entire north
298 Icelandic shelf and extends southwestward to about 63.5°N. The ADT away from the shelf has
299 positive anomalies, and this gradient helps set up a westward anomalous geostrophic current.
300 The anomaly of the surface geostrophic current matches the pattern of the anomalous ADT quite
301 well, suggesting that the NIIC seasonality has a broad spatial scale and coherent variability
302 around Iceland. The maximum anomalous velocity is found to be near the shelfbreak
303 (approximately the 200 m isobath) where the core of the zonal velocity along the Hornbanki
304 section is located. Therefore, the seasonal cycle identified at the Hornbanki section is
305 representative for flows all along the North Icelandic shelf.

306 The horizontal patterns of the temperature and salinity anomalies at 110 m in HYCOM
307 suggest that the North Icelandic shelf has coherent hydrographic changes in March and
308 September (Figs 9 and 10). The peak to peak seasonal change has amplitudes of 8°C in
309 temperature and 0.40 in salinity. The most significant changes in temperature and salinity mainly
310 occur shoreward of the 200-m isobath where the mean hydrographic front is located. The
311 seasonal change in velocity at 200 m from HYCOM is qualitatively similar to that seen in the
312 surface satellite data. The largest variations in velocity at 200 m are found to be near the
313 temperature and salinity front, suggesting that the heat and salt advection by the NIIC may
314 modulate the intensity of the density front and hence affect the baroclinic current near the
315 shelfbreak.

316

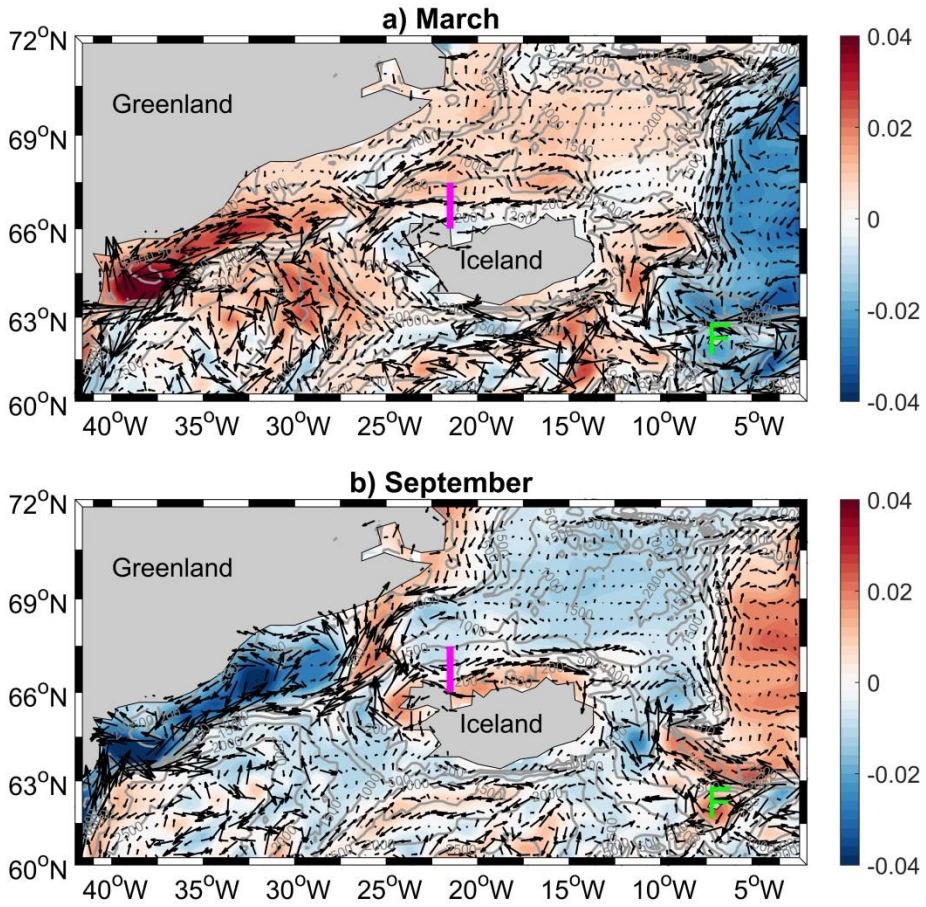

317

318 Figure 8. The anomalous absolute dynamical topography (Unit: m) in March (a) and September
319 (b) corresponding to the minimum and maximum months in the climatological seasonal cycle
320 constructed from the altimetry data. The corresponding surface geostrophic current anomalies are
321 indicated by the vectors. Isobaths are shown in gray lines.

322

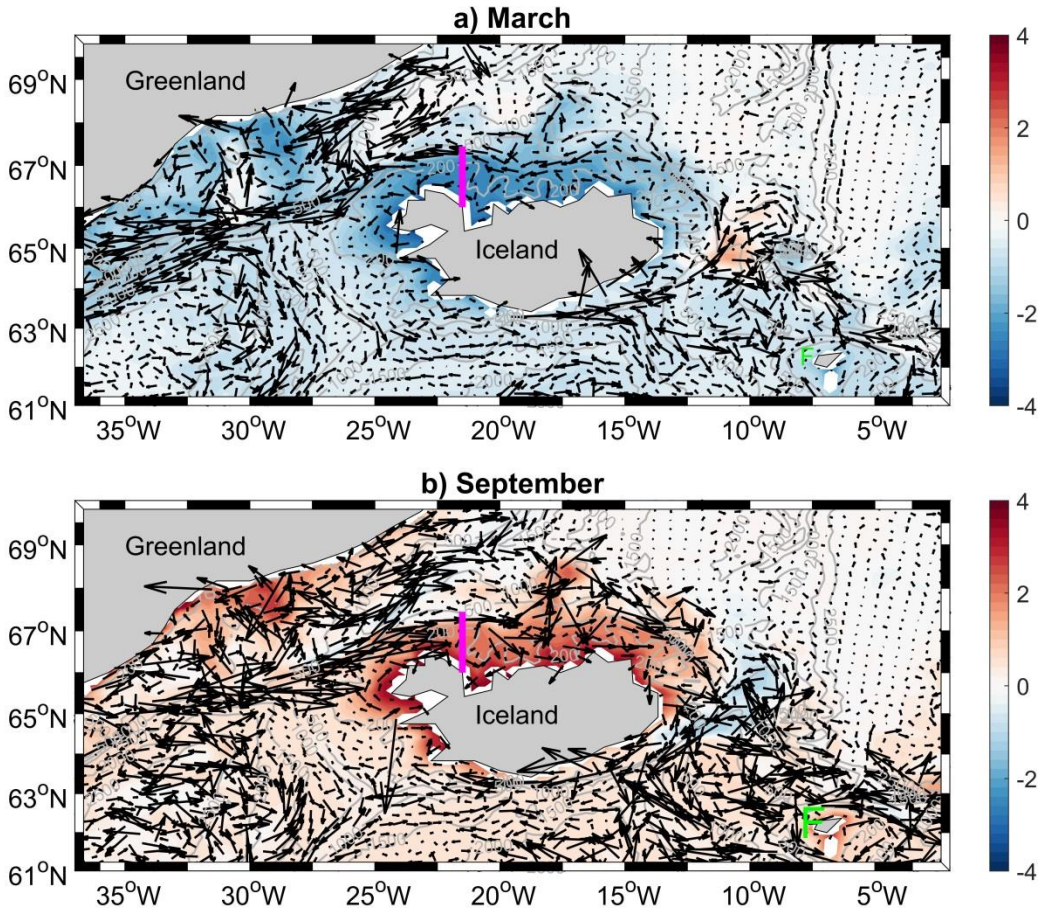

323

324 Figure 9. Temperature anomalies (Unit: ℃) at 110m in March (a) and September (b) from the

325 climatological cycle in the HYCOM *control* run. The corresponding velocity anomalies are

326 indicated by the vectors. Isobaths are shown in gray lines.

327

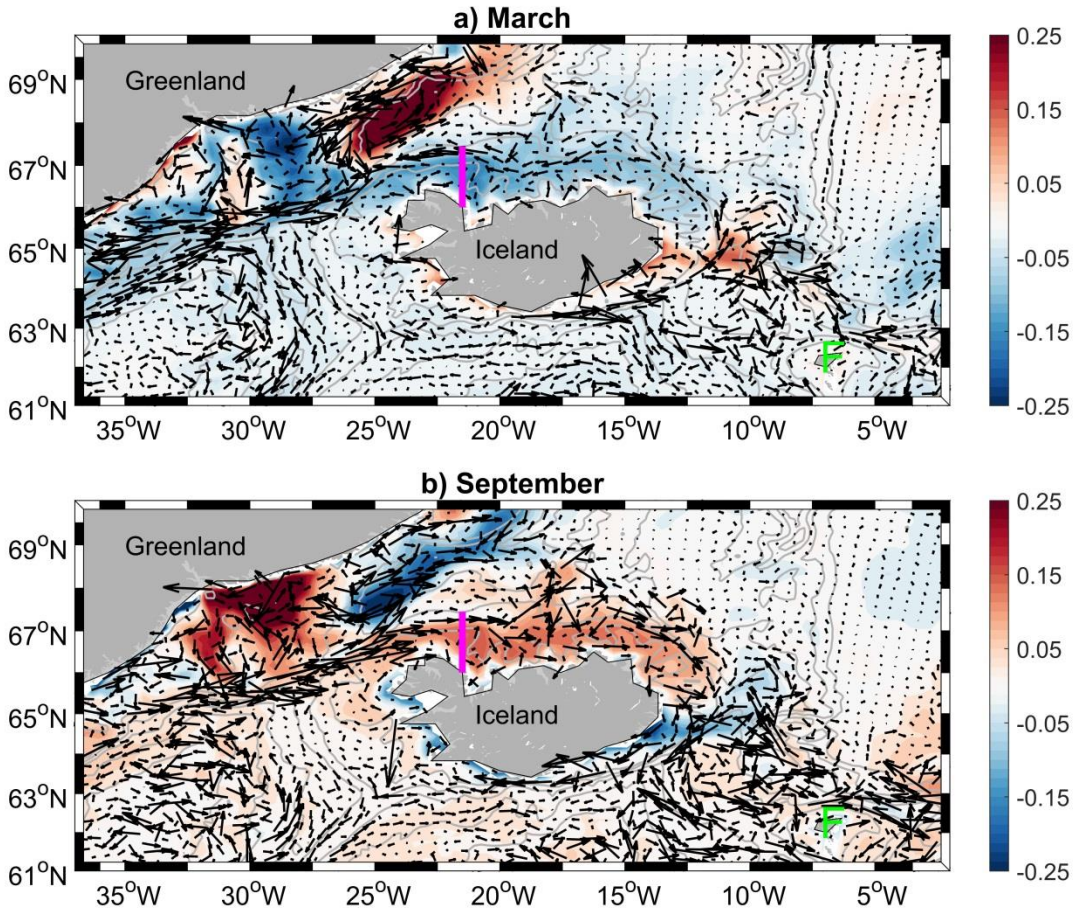

328

329 Figure 10. Same as Fig. 9 except for Salinity anomalies (color shading).

330

331

332

333

334

335

3.2 Interannual variability

The most prominent change in the NIIC over the last two decades is the increase of the AW transport in 2003 (Figs 7a, 11a). The AW volume transport reached a peak value of 1.30 Sv, significantly above the long-term average transport of 0.88 Sv. The event began in late 2002 and lasted until spring 2003, when the climatological AW volume transport should be seasonally low. This event is well simulated in the *control* experiment with a relatively high correlation coefficient of 0.67 between the model and observations. Notably, there is only a small increase in 2003 for the low-pass filtered full NIIC transport (Fig. 7a). The enhancement in the AW transport was accompanied by an increased proportion of AW in the NIIC water, which reaches about 82% in the model and 76% in observations (*Jónsson and Valdimarsson* 2012). For comparison, the proportion of AW for other years is 65%-75% in the HYCOM control run and 53%-67% in the measurements. Thus, the 2003 event clearly stands out from all other years in both AW volume transport and water mass composition.

The elevated proportion of AW resulted in increases in both temperature and salinity of the NIIC water. This is confirmed by the 2-year low-pass filtered temperature and salinity time series at 110 m at 67°N along the Hornbanki section (black curves in Fig.11 b, c). The vertical sections for the temperature and salinity anomalies in 2003 indicate that the most prominent changes took place in the upper 200 m (Fig. 12a and Fig.13a). Similar anomalies in both temperature and salinity are found at the LB6 station (see Fig. 3) where the core AW is located. However, no significant increase in either temperature or salinity is detected at the KG6 station (see Fig. 3) which is predominantly characterized by PW. In addition, the warming event in 2003 was also detected downstream of the Hornbanki section (*Jónsson and Valdimarsson* 2012). Therefore, our analyses indicate that changes observed in 2003 at the Hornbanki section resulted

359 from an increased AW transport along the north Icelandic shelf. The characteristics of this event
360 have been well simulated in our *control* experiment. Therefore, we are confident that our model
361 is suitable for examining the overall interannual variability.

362

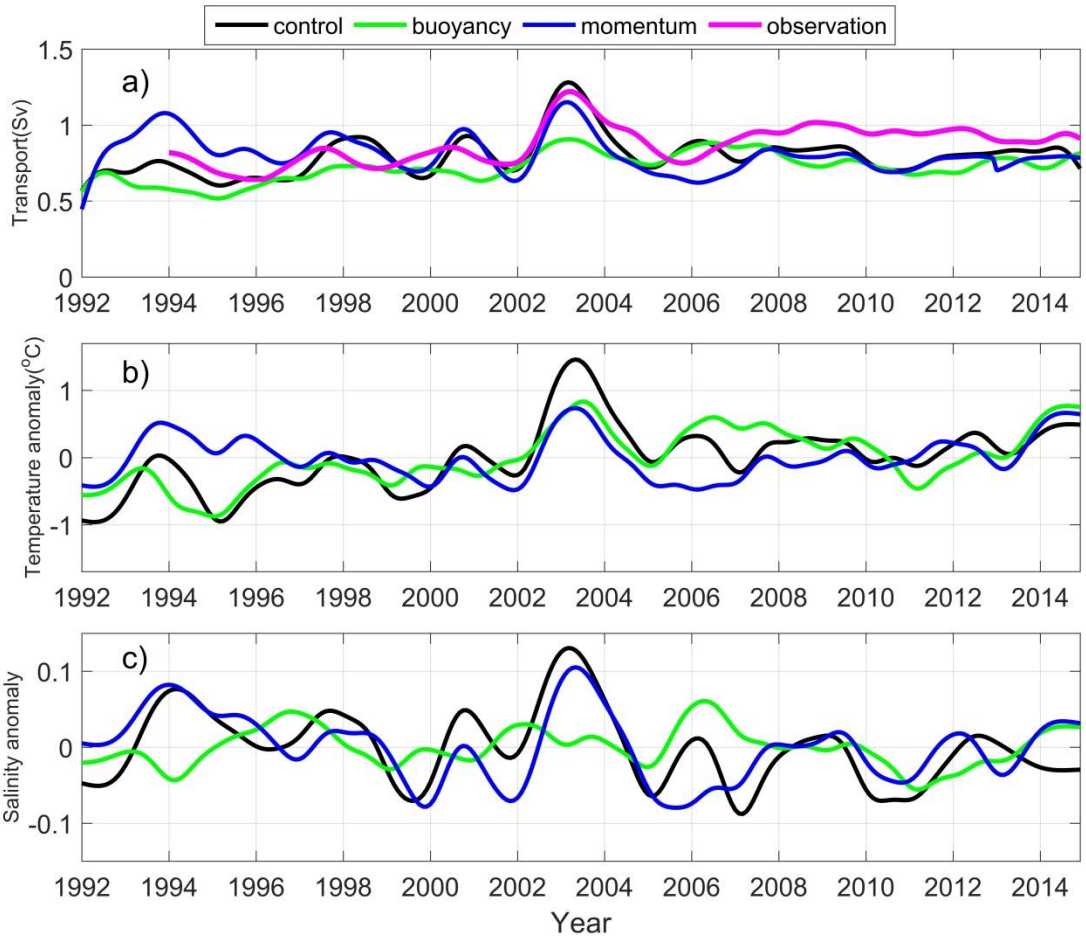

363

364 Figure 11. Interannual anomalies of the AW transport (a), Temperature (b) and salinity (c) at
365 110 m along the Hornbanki section in the control (black), buoyancy (green), and momentum
366 (blue) experiments. The observed AW transport is illustrated by magenta line in panel a).

367

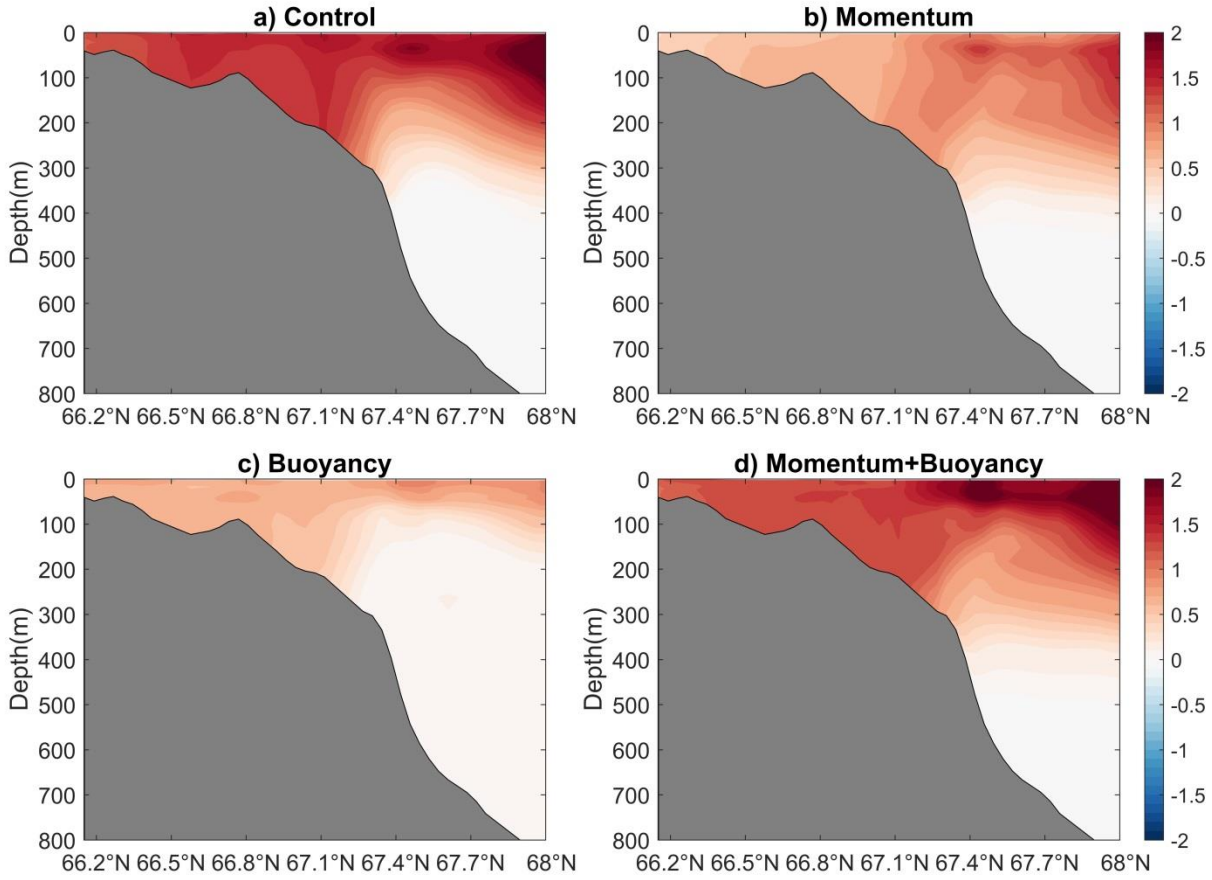

368

369 Figure 12. Temperature anomaly for the Hornbanki section in April 2003 when the largest AW
370 transport in the NIIC occurs (Unit: ℃). The anomaly is calculated from the 2-year low pass
371 filtered data in *Control* (a), *Momentum* (b), and *Buoyancy* (c) runs. The superposition of the
372 anomalies in *momentum* and *buoyancy* experiments are displayed in (d) which recover the
373 *control* results.

374

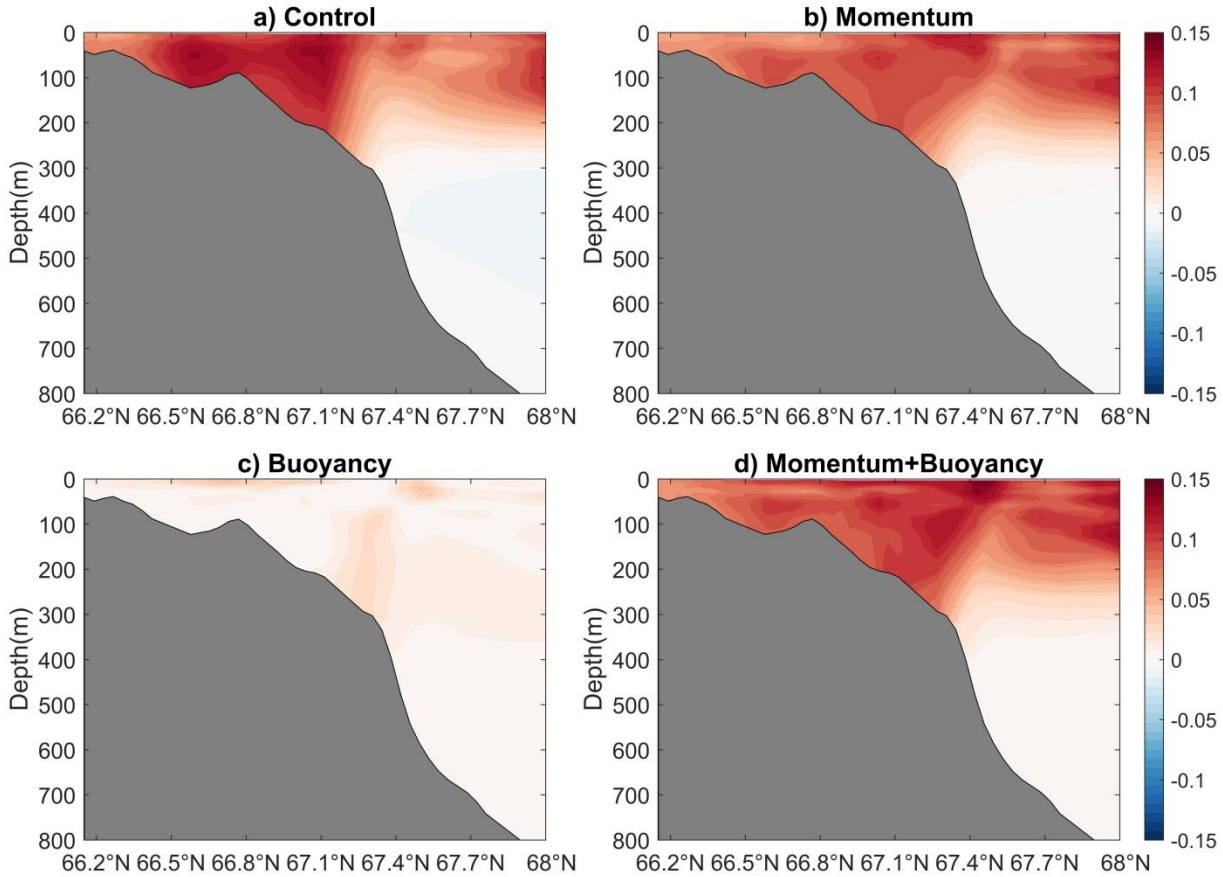

375

376 Figure 13. Same as Figure 12 except for the salinity field.

377

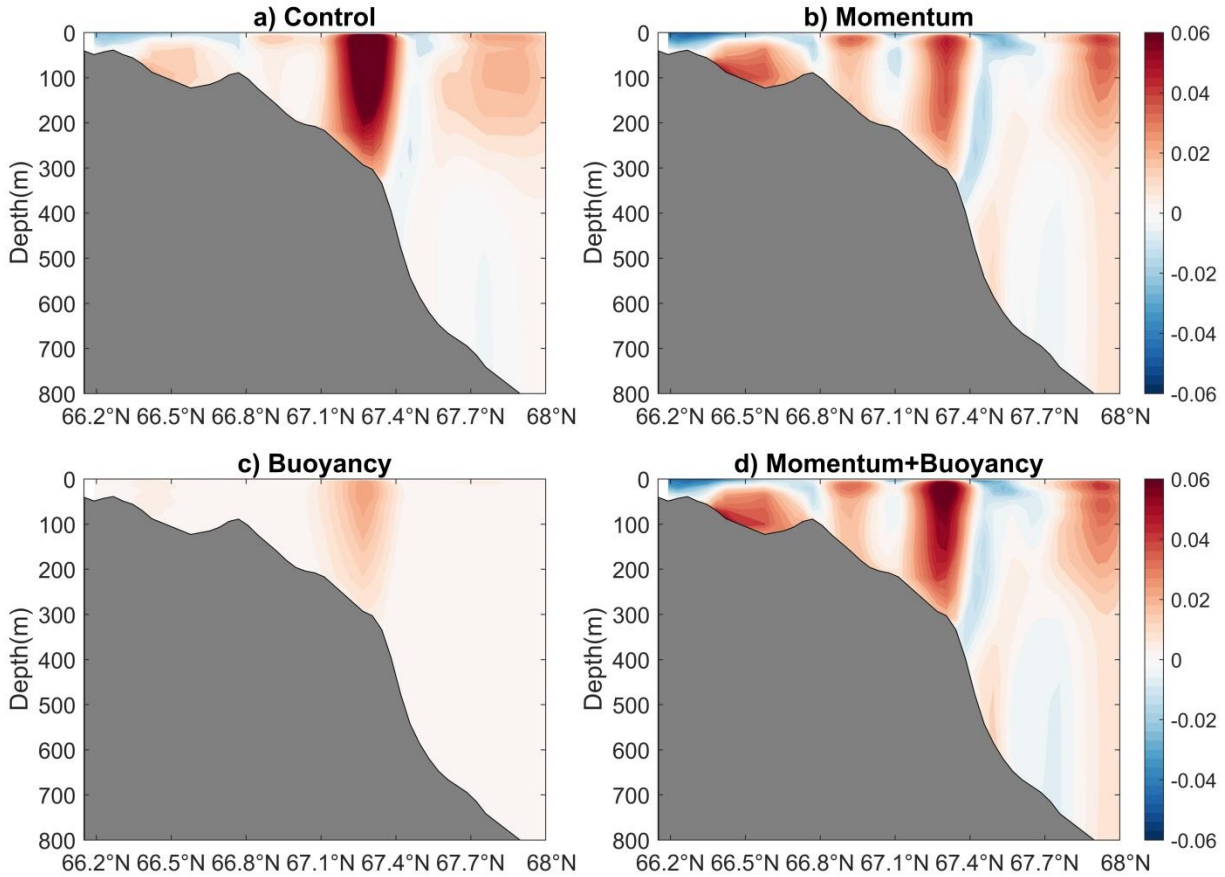

Figure 14, Same as Figure 12 except for the zonal velocity. (Unit: m/s)

To identify the causes for year-to-year changes in the HYCOM *control* run, outputs from the *momentum* and *buoyancy* experiments are analyzed. Note that the seasonal cycles in all three expeirments are quite similar because they share the same climatological seasonal foricng. Their differences are due to interannual forcings.The *momentum* case uses interannually changing wind stress forcing whereas the *buoyancy* experiment is forced by interannually change buoyancy fluxes. The long-term averaged AW transport in the *momentum* run is about 0.87 Sv, virtually identical to 0.88 Sv in the *control* experiment. The *buoyancy* run generates a mean AW transport of 0.78 Sv. The 2-year low-pass filtered AW transport shows that the *momentum* experiment produces interannual changes that closely resemble the *control* run (Fig.11a). In contrast, the AW transport in the *buoyancy* run is relatively steady. Specifically, the intensified AW transport in 2003 reaches a maximum of 1.15 Sv in the *momentum* experiment, but only about 0.90 Sv in the *buoyancy* run. Therefore, the interannual variations in the AW transport are predominately due to the interannually varying momentum fluxes.

The low-pass filtered temperatue time series demonstrate that both the *momentum* and *buoyancy* experiments produce a temperature increase in early 2003. In both experiments, the temperature anomalies at 110 m along the Hornbanki section at 67°N are about 0.6-0.7 ℃ during the 2003 event, which is about half of the 1.4 ℃ in the *control* run. Over the whole simulation period from 1992 to 2014, neither experiment alone can account for the overall interannual changes in temperature that were simulated in the *control* run. The statistical correlation is 0.69 between *momentum* and *control* experiments and is 0.75 between *buoyancy* and *control* runs, both significant at the 95% confidence level.

The temperature anomalies along the Hornbanki section during the maximum AW transport in 2003 show rather different patterns between the *momentum* and *buoyancy* experiments (Fig.12).

More significant changes in the *momentum* run are found to be primarily near the shelfbreak and offshore. The temperature anomaly in the *momentum* experiment reveals a localized region of warming near the shelfbreak that co-locates with the core of the NIIC, indicating that it is likely associated with an intensified AW volume flux.These temperature anomalies help to strengthen the mean temperature front, resulting in a stronger eastward flow. By contrast, the warming generated by the *buoyancy* experiment increases from the outer shelf towards the inner shelf. It is thus evident that changes in buoyancy flux do not significantly affect the AW volume flux and are not responsible for the increased transport in 2003 (Fig. 11a). However, they are partly attributable to temperature anomalies in the shallow waters offshore, which is seen in Figure 12c.

The response in salinity is rather different than that in temperature. The low-pass filtered salinity time series simulated by the *momentum* experiment closely follows that in the *control* run and their correlation is about 0.72, significant at the 95% confidence level (Fig. 11c). The salinity anomalies in both experiments range between -0.1 and 0.14. In contrast, interannual variations in salinity are weak in the *buoyancy* experiment and do not correlate with those in the *control* run (0.05). The vertical section for the salinity anomaly in 2003 reveals that large anomalies are found on the north Icelandic shelf in both the *control* and *momentum* experiments (Fig. 13). In addition, the salinity anomalies in both experiments help to intensify the front near the shelfbreak . The salinity anomalies in the *buoyancy* run are very small almost everywhere along the section, suggesting that the surface buoycancy flux has little impact on the interannual salinity changes. River run-off is included in the model's forcing field. Its freshwater input is only about 0.0048 Sv, and its role in salinity variability is negligible compared with the oceanic transport in this region (*Jonsdottir* 2008). Based on the AW volume fluxes in the *momentum* and *buoyancy* experiments and the salinity pattern shown in Figure 13, we conclude that the

interannual changes for salinity along the Hornbanki section are primarily due to the advection of AW within the NIIC.

The zonal velocity anomalies along the Hornbanki section reveal the spatial structure for the maximum AW transport in 2003 (Fig. 14). Both the *control* and *momentum* experiments generate significant velocity changes over the upper 300 m with elevated amplitude on the shelf, shelfbreak and offshore part of the section. The velocity anomaly in the *buoyancy* run is mostly confined to the shelf break, which is induced by the buoyancy-forced warming signals over the shallow waters. Overall, the velocity responses are consistent with patterns in the temperature and salinity anomalies.

As discussed above, another important factor modulating the AW transport across the Hornbanki section is the relative proportion of AW and PW in the NIIC water. The AW percentages in early 2003 are about 82% and 80% in *control* and *momentum* experiments, respectively. In contrast, the NIIC water in the *buoyancy* run only includes about 68% of the AW, which is the same level as in the climatological state. Therefore, the AW transport in the *buoyancy* run does not have an obvious increase in early 2003 (Fig. 11a).

The premise for comparing the *control*, *momentum* and *buoyancy* experiments is that the physics for the AW interannual variability can be separated into “momentum -driven” and “buoyancy-driven” parts. Despite the inherently nonlinear nature of the ocean circulation, a linear superposition of changes from *buoyancy* and *momentum* forcing largely replicates the temperature, salinity and velocity anomalies in the control experiment (Fig.12d, Fig.13d and Fig.14d). This indicates that the dynamics governing the AW transport are predominantly linear.

3.3 Atmospheric forcing in 2003

To further identify regions where the momentum flux has the largest impact on the AW interannual variability, we computed the statistical correlation between the low-pass filtered AW transport in the *control* run and surface wind stress used in the model. The biggest interannual change, i.e. the 2003 event, only lasted for several months, so that it is difficult to reveal any time lags between the atmospheric forcing and oceanic response using monthly time series. This study is therefore trying to identify the important regions to affect the NIIC and its AW transport. The long-term mean surface wind stress exhibits a cyclonic circulation associated with the Icelandic Low (Fig. 15a). The regressions of zonal and wind stress onto the AW transport leads to a spatial pattern that is quite similar to the long-term field (Fig. 15b). The statistically important regions can be found from the correlation between the AW transport and the wind stress magnitude. The regions passing the 95% confidence level of the Student's t test are the eastern coast of Greenland, the northern Irminger Sea, as well as the area adjacent to southwest Iceland. Since the PW at the KG6 station does not show substantial interannual variability in temperature and salinity, the wind forcing off Greenland is less likely to be responsible for changes of the AW transport across the Hornbanki section. The increased southeasterly wind parallel to the southwest coast of Iceland leads to onshore Ekman transport and consequently produces northward geostrophic flow. The changes in pressure gradient and geostrophic velocity would propagate to the Hornbanki section and enhance the AW transport. These processes either in barotropic or baroclinic occur on relatively short time scale, usually less than 1 month (*Richter et al.* 2009). It is therefore difficult to capture them by lead-lag correlations of monthly data. In addition, the intensified easterly wind in the northern Irminger Sea would enhance the Irminger Current and hence increase the part that feeds the NIIC. Therefore, it appears more likely that the

wind forcing southwest of Iceland and in the northern Irminger are responsible for the interannual variability of AW transport along the Hornbanki section.

To further elucidate the role of the wind field in the 2003 anomaly of AW transport in the NIIC, we examined the Sea Level Pressure (SLP) field from the monthly NCEP-CFSR dataset. The climatological mean SLP from January to April is constructed from the monthly data between 1992 and 2015. As shown in Fig.16a, the Icelandic Low is centered in the Irminger Sea, and in the Nordic Seas there is a signature of the Lofoten Low (in the northeastern-most part of the domain). In contrast, the mean SLP between January and April in 2003 indicates that the Icelandic Low deepened considerably and expanded into the Labrador Sea (Fig. 16b). The low pressure in the Nordic Seas also weakened. Taking the difference between the mean SLP in Jan.-Apr. 2003 and its corresponding climatological field yields the SLP anomaly pattern in early 2003 (Fig.16c). The SLP anomaly reveals a strong dipole, with a low centered near the southern tip of Greenland and a high located in the eastern Norwegian Sea. This large scale SLP anomaly is associated with strengthened southeasterly winds off the southwest coast of Iceland, which in turn would result in more AW advected onto the north Icelandic shelf.

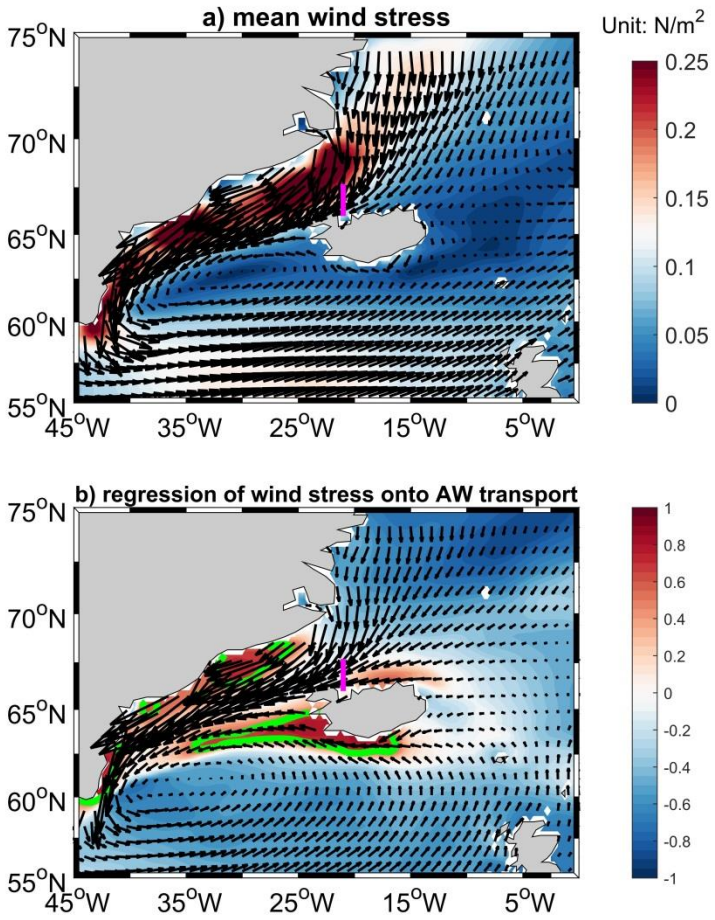

493

494

495 Figure 15. a) Mean (1992-2015) surface wind stress from the CFSR dataset is displayed in
496 vectors and its magnitude is in color shading. b) Regression of low-pass filtered wind stress onto
497 the low-pass filtered AW transport in the *control* run. The correlation between the AW transport
498 and the wind stress magnitude is displayed in color shading. The green lines mark the region
499 where the confidence level exceeds 95% in the Student's t-test.

500

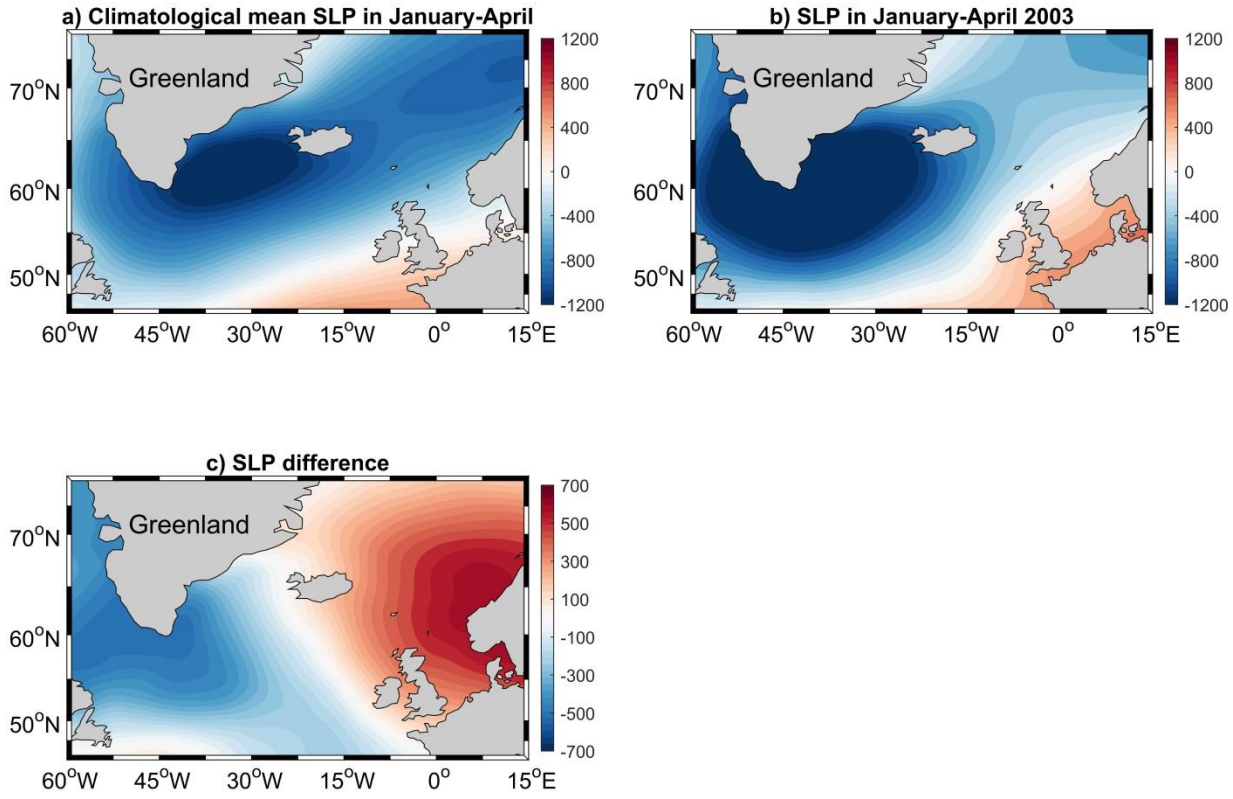

501

502

503 Figure 16. a) Climatological mean sea level pressure (SLP) from January to April for the time
504 period 1992 – 2015. b) Mean SLP field between January and April 2003. c) The 2003 mean
505 field minus the climatological mean field. In panels a) and b), a reference value for the mean sea
506 level pressure (1.01325×10^5 Pa) is removed from the original data. Unit: Pa.

507

508

509

4 Summary and Discussion

In this study we have used the high-resolution HYCOM numerical model, together with various data sources, to investigate the seasonal to interannual variability of the North Icelandic Irminger Current (NIIC) and its AW transport. The mean hydrography and velocity structure along the Hornbanki section north of Iceland are well reproduced by HYCOM. Consistent with observations, the model shows that the warm and salty water in the NIIC occupies the north Icelandic shelf and helps maintain a hydrographic front near the shelfbreak. The NIIC velocity profiles have both strong barotropic and baroclinic components. The core of the current is near the shelfbreak, corresponding to the density front.

The water mass in the NIIC is a mixture of Atlantic water (AW) and polar water (PW) and their ratios at the Hornbanki section were estimated using two end-member hydrographic profiles, as has been done in previous observational studies. The fraction of AW ranges from 50% to 95%, yielding a mean value of 72%. This value is slightly higher than the 66% obtained from the observations of *Jónsson and Valdimarsson* (2005). The mean AW transport in the model, as well as the simulated seasonal cycle and interannual variability, compare well with that from observations. This reveals that the essential dynamics governing the flow of AW are well represented in the model.

The volume flux of AW in the NIIC varies considerably with season, from a minimum in late winter and early spring to a maximum in early fall. Variability in the relative percentages of the AW and PW contributes significantly to the NIIC seasonal cycle. The AW fraction changes seasonally in coherence with the AW volume transport. The seasonal changes of the

hydrographic structure over the entire north Icelandic shelf are in turn strongly modulated by this transport.

The most significant interannual change along the Hornbanki section in the two decades considered here occurred in 2003 and was related to the enhancement of the AW transport by the NIIC. This event is captured well in our control experiment. Two additional experiments were conducted to separate the impacts of buoyancy and momentum fluxes on the NIIC. Changes in wind stress alone, as shown in the *momentum* experiment, are largely responsible for the interannual variations in the AW volume transport and salinity. Variations in temperature, however, are attributed almost equally to changes in surface wind stress and buoyancy fluxes. Our analyses show that the two forcing fields affect the temperature through different processes. The wind-driven AW transport brings warm water onto the shelf and consequently impacts the temperature near the shelfbreak. The buoyancy forcing generates a temperature anomaly through surface forcing, with signals mainly located on the shelf and in the surface layer offshore.

Further statistical analyses between the AW volume transport and surface wind stress reveal that it is the wind stress southwest of the Iceland that seems to be primarily responsible for the interannual variability of the AW transport. Intensified southeasterly winds strengthen the NIIC transport of the AW to the north Icelandic shelf. This is consistent with the composite analyses conducted by *Richter et al.* (2009) who showed that the NIIC transport correlates positively with southerly wind anomalies around Iceland.

Previous studies pointed out that the wind-stress forcing is primarily responsible for salinity anomalies entering the Nordic Seas (*Hátún* et al. 2005; *Häkkinen* et al. 2011). Weakening cyclonic wind stress curl in the subpolar North Atlantic renders a westward shift of the subpolar

front, so that more warm and saline subtropical waters penetrate farther north in the eastern sub-basin and hence increase the salinity in the inflow to the Nordic Seas. The most striking feature for the wind-stress curl over the subpolar gyre is a decreasing trend starting from the 1990s. It qualitatively agrees with the increasing trend detected from the observed salinity time series along the Kögur section to the west of the Hornbanki line (*Pickart et al.* 2017). The numerical results in this study do not generate a long-term trend, at least not along the Hornbanki section. Instead, the most important interannual changes are the increased AW transport and hydrographic signals in 2003. They are attributed to the wind forcing southwest of Iceland generated by the strengthening and westward shift of the Icelandic Low in early 2003. Although the local wind around Iceland is affected by the large scale atmospheric pattern in the subpolar gyre, the different behaviors in the salinity time series suggest that the interannual variability discussed here is different from the long-term trend in the large-scale forcing.

Acknowledgement:

This work is supported by the U.S. National Science Foundation (NSF) under Grants OCE-1634886 (J. Zhao and J. Yang) and OCE-1558742 (R. Pickart), and by the Bergen Research Foundation Grant BFS2016REK01 (K. Våge and S. Semper). We thank Xiaobiao Xu at Florida State University for providing the initial model configuration. The altimeter products are produced and distributed by the Copernicus Marine and Environment Monitoring Service (CMEMS) (http://www.marine.copernicus.eu). The hydrographic maps along the Hornbanki section are available at http://www.hafro.is/Sjora/

References:

Behrens, E., K. Våge, B. Harden, A. Biastoch, C.W. Böning, (2017), Composition and variability of the Denmark Strait Overflow Water in a high-resolution numerical model hindcast simulation. Journal of Geophysical Research, 122, 2830–2846, doi:10.1002/2016JC012158

Dickson, R. R., and J.Brown (1994), The production of North Atlantic Deep Water: Sources, rates, and pathways, J. Geophys. Res., 99(C6), 12319–12341, doi:10.1029/94JC00530.

Dickson, R., J. Meincke and P. Rhines (2008), Arctic-Subarctic Ocean Fluxes, Springer, pp736

Häkkinen, S., P. B. Rhines and D. L. Worthen (2011), Warm and saline events embedded in the meridional circulation of the northern North Atlantic, J. Geophys. Res., 116, C03006, doi:10.1029/2010JC006275.

Hansen B. and S. Østerhus, (2000), North Atlantic–Nordic Seas exchanges, Progress in Oceanography, 45, 109-208.

Hansen, B., S. Østerhus, H. Ha´tu´n, R. Kristiansen, and K. M. H. Larsen (2003), The Iceland-Faroe inflow of Atlantic water to the Nordic Seas, Prog. Oceanogr., 59, 443–474.

Hansen, B., Østerhus, S., Turrell, B., Jónsson, S., Valdimarsson, H., Hátún, H., Olsen, S.M. 2008. The inflow of Atlantic water, heat, and salt to the Nordic Seas across the Greenland-Scotland Ridge. In Arctic–Subarctic Ocean Fluxes: Defining the role of the Northern Seas in Climate, 15 - 43 (eds Dickson, D., Meincke, J. & Rhines, P.), Ch. 1, Springer Science + Business Media B.V., 15-43.

Hansen, B., H. Hátún, R. Kristiansen, S. M. Olsen, and S. Østerhus, 2010: Stability and forcing of the Iceland–Faroe inflow of water, heat, and salt to the Arctic, Ocean Sci., 6, 1245–1287.

Hansen, B. K. M. H. Larsen, H. Hátún, R. Kristiansen, E. Mortensen and S. Østerhus, 2015: Transport of volume, heat and salt towards the Arctic in the Faroe Current 1993-2013. Ocean Sci., 11, 743-757, doi:10.5194/os-11-743-2015.

Hátún, H., B. Hansen, A. B. Sandø, H. Drange, and H. Valdimarsson (2005), De-stabilization of the North Atlantic Thermohaline Circulation by a gyre mode, Science, 309, 1841–1844.

Jakobsen, P. K., M. H. Ribergaard, D. Quadfasel, T. Schmith, and C. W. Hughes (2003), Near-surface circulation in the northern North Atlantic as inferred from Lagrangian drifters: Variability from the mesoscale to interannual, J. Geophys. Res., 108, 3251, doi:10.1029/2002JC001554, C8.

Jónsson, S. (1999), The circulation in the northern part of the Denmark Strait and its variability, ICES CM, L:06, 9 pp

Jónsson, S., and Valdimarsson, H. 2004. A new path for the Denmark Strait Overflow Water from the Iceland Sea to Denmark Strait. Geophysical Research Letters, 31: L03305

Jónsson, S. and H. Valdimarsson, (2005), The flow of Atlantic water to the North Icelandic Shelf and its relation to the drift of cod larvae. ICES Journal of Marine Science, 62, 1350-1359, doi:10.1016/j.icesjms.2005.05.003

Jónsson, S. and H. Valdimarsson, (2012), Water mass transport variability to the north Icelandic shelf, 1994-2010.ICES Journal of Marine Science, doi:10.1093/icesjms/fss024.

Kristmannsson, S. S. (1998), Flow of Atlantic water into the northern Icelandic shelf area, 1985–1989. ICES Cooperative Research Report, 225: 124–135

Logemann, K., and Harms, I. (2006) High resolution modelling of the North Icelandic Irminger current (NIIC). Oc. Sci. Discussions, 3:1149-1189.

633 Nilsen, J. E. Ø., Y. Gao, H. Drange, T. Furevik, and M. Bentsen, 2003: Simulated North
634 Atlantic–Nordic seas water mass exchanges in an isopycnic coordinate OGCM, Geophys. Res.
635 Lett., 30(10), 1536, doi:10.1029/2002GL016597.

636

637 Olsen, S. M. and T. Schmith, 2007: North Atlantic-Arctic Mediterranean exchanges in an
638 ensemble hincast experiment. J. Geophys. Res., 112, C04010, doi:10.1029/ 2006JC003838.

639

640 Orvik, K. A., and Ø. Skagseth, 2003: The impact of the wind stress curl in the North Atlantic on

641 the Atlantic inflow to the Norwegian Sea toward the Arctic, Geophys. Res. Lett., 30(17), 1884,
642 doi:10.1029/2003GL017932.

643

644 Østerhus, S., Turrell, W. R., J´onsson, S., and Hansen, B., 2005: Measured volume, heat, and salt

645 fluxes from the Atlantic to the Arctic Mediterranean, Geophys. Res. Lett., 32, L07603,
646 doi:10.1029/2004GL022188.

647

648 Pickart, R. S., M. A. Spall, D. J. Torres, K. Vage, H. Valdimarsson, C. Nobre, G. W. K. Moore,
649 S. Jonsson, and D. Mastropole, 2017. The North Icelandic Jet and its relationship to the North
650 Icelandic Irminger Current. Journal of Marine Research, 75, 605-639.

651

652 Richter, K., T. Furevik, and K. A. Orvik, 2009: Effect of wintertime low pressure systems on the

653 Atlantic inflow to the Nordic seas, J. Geophys. Res., 114, C09006, doi:10.1029/2009JC005392.

654

655 Richter K, Segtnan O and Furevik T, 2012: Variability of the Atlantic inflow to the Nordic Seas

656 and its causes inferred from observations of sea surface height J. Geophys. Res.: Oceans,

657 117, C04004, doi:10.1029/2011JC007719

658

659 Sandø, A. B., and T. Furevik, 2008: Relation between the wind stress curl in the North Atlantic

and the Atlantic inflow to the Nordic Seas, J. Geophys. Res., 113, C06028, doi:10.1029/2007JC004236.

Sandø, A. B., J. Nilsen, T. Eldevik and M. Bentsen, 2012: Mechanisms for variable North Atlantic-Nordic seas exchanges, J. Geophys. Res., 117, doi:1029/ 2012JC008177

Sherwin, T. J., S. L. Hughes, W. R. Turrell, B. Hansen and S. Østerhus, 2008: Wind-driven monthly variations in transport and the flow field in the Faroe-Shetland Channel. Polar Research, 27, 7-22.

Skjoldal, H. (Ed.) (2004), The Norwegian Sea Ecosystem, 560 pp., TapirAkad. Forlag, Trondheim, Norway

Thordardottir, Th. 1984. Primary production north of Iceland in relation to water masses in May–June 1970–1980. ICES Document CM 1984/L: 20. 17 pp.

Våge, K., R. S. Pickart, M.A. Spall, H. Valdimarsson, S. Jonsson, D.J. Torres, S. Osterhus, T. Eldevik, (2011), Significant role of the North Icelandic Jet in the formation of Denmark Strait Overflow Water, Nature Geosci., 4 723-727. doi:10.1038/ngeo1234

Våge, Kjetil, R. S. Pickart, M. A. Spall, G. W. K. Moore, H. Valdimarsson, D. J. Torres, S. Y. Erofeeva, and J. E. O. Nilsen, 2013: Revised circulation scheme north of the Denmark Strait. Deep Sea Research I, 79, 20-39.

Valdimarsson, H. and S.-A. Malmberg, 1999. Near-surface circulation in Icelandic waters derived from satellite tracked drifters. Rit Fiskideildar, 16, 23–39.

687 Xu, X., W. J. Schmitz Jr., H. E. Hurlburt, P. J. Hogan, and E. P. Chassignet, 2010, Transport of
688 Nordic Seas overflow water into and within the Irminger Sea: An eddy-resolving simulation and
689 observations, J. Geophys. Res. Oceans, 115, C12048, doi:10.1029/ 2010JC006351.

690

691 Xu, X., W. J. Schmitz Jr., H. E. Hurlburt, and P. J. Hogan (2012), Mean Atlantic meridional
692 overturning circulation across 26.5°N from eddy-resolving simulations compared to observations,
693 J. Geophys. Res., 117, C03042, doi:10.1029/2011JC007586.

694

695 Xu, X., H. E. Hurlburt, W. J. Schmitz Jr., J. Fischer, R. Zantopp, and P. J. Hogan, 2013, On the
696 currents and transports connected with the Atlantic meridional overturning circulation in the
697 subpolar North Atlantic, J. Geophys. Res. Oceans, 118, doi:10.1002/jgrc.20065.